Mapping the Aftermath of the DANA Flood: Supporting Urban Disaster Response Through Post-Flood Extent Estimation

Emanuele Alcaras[1], Paola Mercogliano[2]

[1]Department of Department of Science and Technology, Parthenope University of Naples, 80143 Naples, Italy
emanuele.alcaras@uniparthenope.it
[2]CMCC Foundation - Euro-Mediterranean Center on Climate Change, Italy
paola.mercogliano@cmcc.it

Keywords: GIS, Remote Sensing, Geospatial Analysis, Floods, Mapping, Disaster.

Abstract

In October 2024, southeastern Spain was severely impacted by the DANA (Depresión Aislada en Niveles Altos), a high-intensity weather event that triggered extensive flooding, disrupted infrastructure, and caused major damage across both urban and rural landscapes. Rapid and accurate mapping of flood extent is critical to support emergency management efforts and inform mitigation strategies. This study focuses on a highly vulnerable area near Valencia, where the goal is to map with maximum precision the flooded zones located within the defined study boundaries. For this purpose, the effectiveness of five spectral indices commonly used for flood detection is evaluated: the Normalized Difference Water Index (NDWI), the Modified NDWI (MNDWI), the Automated Water Extraction Index (AWEI), the Normalized Difference Flood Index (NDFI), and the recently introduced Flood Mud Index (FMI), which is specifically designed to detect sediment-rich waters. The indices are calculated using Landsat-8 imagery acquired shortly after the DANA event. A supervised classification is then performed using the Maximum Likelihood Classification algorithm to separate flooded and non-flooded covered areas for each index. The analysis revealed significant differences in the capacity of each index to delineate flood extent, especially in turbid waters, where traditional indices tend to underperform. Among all tested methods, the FMI consistently produced the most accurate and spatially coherent results. The FMI achieved an Overall Accuracy of 0.9764 and identified a flooded area of 4081.490 hectares. These outcomes emphasize the importance of selecting suitable spectral tools based on floodwater characteristics and demonstrate how remote sensing methods can play a key role in supporting urban disaster response and recovery following extreme events such as DANA.

1. Introduction

Extreme weather events, particularly those associated with intense rainfall, are becoming increasingly frequent and severe in the Mediterranean region (Nissen and Ulbrich, 2017), identified by the IPCC AR6 as a climate change hotspot (IPCC, 2022). A catastrophic storm occurred in October 2024, when extreme rainfall struck the city of Valencia and its surrounding areas (Astaburuaga, 2025) with devastating consequences, associated with a DANA (Depresión Aislada en Niveles Altos). Specifically, this event caused extensive damage to infrastructure, widespread flooding, and significant social and economic losses (Martin-Morero et al, 2025), leading to the death of over 200 people (Morote et al., 2025).

In situations like this, it is crucial to quickly assess and map the extent of flooded areas to support emergency response and recovery efforts. However, on-site surveys are not always feasible due to safety concerns, limited accessibility, and high operational costs during or immediately after such disasters.

Remote sensing techniques offer a valuable solution in such contexts, as they eliminate the need for in-situ operators (Alcaras and Vallario, 2025), enable rapid assessments, and are generally cost-effective (Rahaman and Di, 2017). Many of these techniques rely on multispectral sensors, which capture image data across multiple bands of the electromagnetic spectrum, including visible and near-infrared wavelengths (Albertini et al., 2022). These sensors allow analysts to exploit the distinct spectral signatures of different surface materials (Rencz and Ryerson, 1999)—such as water, vegetation, soil, and built-up areas—to differentiate between flooded and non-flooded regions. Floodwaters, particularly those laden with sediment, exhibit unique reflectance properties that can be detected and mapped using appropriate spectral indices (Munawar et al., 2022).

In addition to spectral analysis, change detection techniques are commonly employed in flood mapping (Aggarwal et al., 2016) (Huang and Jin, 2020) (Ramola and Vidyarthi, 2024). These methods involve comparing satellite images acquired before and after a flood event to identify significant changes in surface characteristics. By detecting alterations in spectral reflectance patterns, analysts can delineate the extent of flood-affected areas (Moya et al., 2019). However, this approach requires cloud-free pre-event imagery, which is not always available in emergency situations, highlighting the need for reliable single-date methods.

To enable the accurate classification of flooded and non-flooded areas, machine learning techniques are often employed (Munawar et al., 2021). These methods rely on a training phase, during which the algorithm learns to recognize the spectral characteristics associated with each class based on labelled input data (training samples) (Muñoz-Marí, et al., 2007). Once trained, the classifier is able to automatically assign each pixel in the image to one of the predefined classes—flooded or non-flooded—based on its spectral properties (Sisodia et al., 2014). This process enhances classification accuracy and significantly reduces the time required for manual interpretation (Alcaras et al., 2025), which is critical in time-sensitive post-disaster scenarios.

When working with single-date datasets, it becomes especially important to maximize the spectral contrast between the two target classes—flooded and non-flooded areas. Several spectral indices have been proposed in the literature to identify water

bodies (Bijeesh and Narasimhamurthy, 2020), and these are frequently applied for flood detection purposes (Samela et al., 2022). However, identifying the most suitable index is not straightforward, as performance can vary significantly depending on the specific context. A preliminary analysis is often necessary to determine which method provides the highest level of classification accuracy.

The effectiveness of a given index depends on various factors, including the characteristics of the sensor—particularly the wavelengths it captures—as well as the properties of the observed scene (Teillet et al., 1997). The presence of pre-existing water bodies, the type and concentration of suspended sediments, shadows, vegetation cover, and other environmental elements can all influence index performance.

The aim of this study is to map the extent of flooded areas resulting from the DANA event that struck the province of Valencia in October 2024. To achieve this, several spectral indices from the literature are applied and compared. Their performance is evaluated in terms of classification accuracy, and particular attention is given to assessing the degree to which each index overestimates or underestimates the extent of flooding.

2. Materials and Methods

The methodology adopted in this study follows the workflow illustrated in Figure 1. After the initial preprocessing of the satellite imagery, several spectral indices are computed. These indices are then subjected to supervised classification using the Maximum Likelihood Classification algorithm. Then, the classification outputs are evaluated through accuracy assessment and compared to highlight the relative performance of each index. Finally, the extension of the flood is determined.

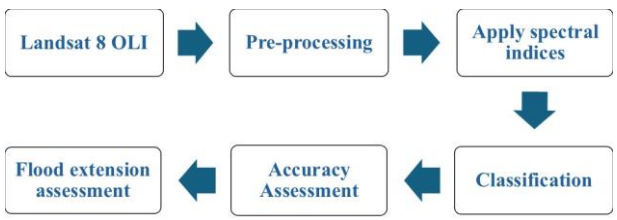

Figure 1. Flowchart of the methodology.

2.1 Study Area

The study area is located in the eastern part of Spain, within the Valencian Community, as shown in Figure 2.

Figure 2. Geolocalization of the study area in eastern Spain (in red), in equirectangular projection and WGS84 geographic coordinates.

The study area is crossed by two main rivers: the Turia, which flows through the city of Valencia, and the Júcar, located further south (Carmona González and Ruiz Pérez, 2000). Also to the south lies the Parque Natural de la Albufera, a large coastal lagoon separated from the Mediterranean Sea by a narrow strip of land (Soria et al., 2021).

South of Valencia, there is an important agricultural zone, particularly dedicated to rice cultivation. The area is also characterized by the presence of citrus orchards, vegetable gardens, and greenhouses (Argyelan et al., 2015).

The coastal region is predominantly flat, with fertile alluvial soils that are highly prone to waterlogging and surface flooding (Eguibar et al., 2021).

Valencia itself is a densely urbanized city, surrounded by rapidly expanding peri-urban areas (Garcia, 2013). Some of the urban zones are located near water bodies or even below sea level, making them particularly vulnerable to flooding (Çal and Ciravoğlu, 2024).

2.2 Dataset

In this study, we used a Level-1 Landsat 8 OLI dataset (U.S. Geological Survey, 2019). The imagery was acquired on October 30th, 2024, just one day after the flooding event. The captured scene includes the city of Valencia and extends up to 40 km south of the urban area.

Figure 3 displays an RGB composite of the dataset, where flooded areas are visible in brown, highlighting the extent of the water coverage in the aftermath of the event.

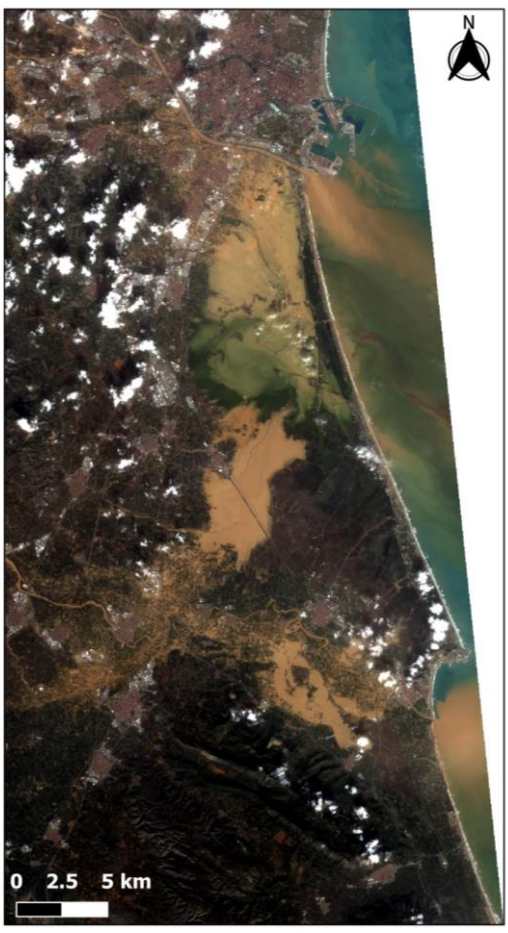

Figure 3. RGB true colour composition of the Landsat 8 OLI images, flooded areas are clearly visible in brownish colour.

2.3 Supervised Classification

Supervised classification operates by partitioning the spectral field into regions corresponding to specific land cover classes relevant to the study objective (Richards, 2013). This approach requires prior knowledge of the scene, typically obtained through the careful selection of representative training samples to ensure accurate classification results (Liu, 2005).
In this study, the Maximum Likelihood Classification (MLC) method is employed. Rooted in Bayesian probability theory, MLC is widely regarded in the literature as one of the most effective classification techniques—particularly when high-quality training data are available (Perumal and Bhaskaran, 2010). Training samples, in this work, are representative of flooded and non-flooded areas. Training samples cover about 1500 pixels per class.
MLC is particularly robust and effective in low complexity studies like this one, searching for only two classes (Mianji and Zhang, 2011). Furthermore, using MLC enabled a direct comparison with existing literature, ensuring that the performance of the indices can be fairly evaluated through a well-established classification approach.
In this study MLC is applied to classify each index.

2.4 Indices

In this work five indices known in literature (Normalized Difference Water Index, Modified Normalized Difference Water Index, Automated Water Extraction Index, Normalized Difference Flood Index, and Flood Mud Index) are applied and then described in the following. These indices are among the most employed for the detection of flooding from remotely sensed images.
The Normalized Difference Water Index (NDWI) leverages the green and near-infrared bands to enhance the contrast between water and land (McFeeters, 1996):

$$NDWI = \frac{Green - NIR}{Green + NIR} \quad (1)$$

A modified version of NDWI (MNDWI) was later proposed (Xu, 2006), using the short-infrared band instead of the near-infrared one:

$$MNDWI = \frac{Green - SWIR2}{Green + SWIR2} \quad (2)$$

One of the most commonly used indices for flood detection is the Automated Water Extraction Index (AWEI), which was specifically developed to improve water body extraction in areas with significant urban influence (Feyisa et al., 2014):

$$AWEI=4*(Green - SWIR2) - (0.25*NIR + 2.75 * SWIR1) \quad (3)$$

The Normalized Difference Flood Index (NDFI), on the other hand, was specifically developed to map flooded areas by leveraging the reflectance differences between the blue and shortwave infrared bands (Wan and Billa, 2018):

$$NDFI = \frac{Blue - SWIR2}{Blue + SWIR2} \quad (4)$$

Finally, the Flood Mud Index (FMI) was developed specifically for flooded areas with high water turbidity, leveraging blue and red bands (Alcaras, 2025):

$$FMI = \frac{Red - Blue}{Red + Blue} \quad (5)$$

2.5 Accuracy Evaluation

Accuracy assessment is conducted using a set of test sites. It is important to note that these test sites are separate from the training samples but are likewise representative of the two target classes: flooded and non-flooded areas (Story and Congalton, 1986). Test sites cover about 1000 pixels per class.
To evaluate the thematic accuracy of the classification methods adopted, the Overall Accuracy (OA) metric is used. OA reflects the proportion of pixels correctly classified into the two selected classes (Liu et al., 2007).
Finally, the area estimation is performed using the $area command available in the free and open-source software Quantum GIS (QGIS) (Quantum GIS, 2025).

3. Results and Discussion

The results presented and discussed below have been processed using specific masks. In particular, masks were applied to filter out clouds and sea areas. Moreover, pre-existing water bodies (e.g., rivers) and the wetlands of the Albufera were excluded using official cartographic data provided by the Spanish government.
Table 1 shows the results obtained by calculating the Overall Accuracy for each index. The optimal value for the Overall Accuracy is equal to 1.

Method	Overall Accuracy
NDWI	0.5021
MNDWI	0.7857
AWEI	0.8229
NDFI	0.7450
FMI	0.9764

Table 1. Overall Accuracy values for each index.

The results presented in Table 1 reveal three distinct levels of thematic accuracy. The NDWI proves unsuitable for flood area detection in this specific context, as indicated by its very low Overall Accuracy (OA). In contrast, the NDFI, MNDWI, and AWEI yield significantly better outcomes, with the latter achieving a relatively high OA value. Finally, the OA obtained with the FMI is by far the highest among all methods evaluated, clearly confirming FMI as the most effective index in this study. Considering the results obtained, the flooded areas identified by the FMI will be taken as the reference for subsequent analyses.
Table 2 reports the total area (in hectares) identified as flooded by each spectral index, allowing a comparative assessment of their spatial outputs.

Method	Area (hectares)
NDWI	255.028
MNDWI	14635.704
AWEI	6705.044
NDFI	16441.449
FMI	4081.490

Table 2. Extent of the flooded areas as achieved by each index.

According to the classification performed using the FMI, the flooded surface area is estimated to be 4,081.490 hectares, as

shown in Table 2. This value will serve as the reference extent for the purposes of this study.

In this regard, taking into account the values in Table 2, a preliminary comparison with the results obtained from the other indices can be conducted. Notably, the NDWI significantly underestimates the extent of flooded areas. In contrast, the remaining three indices tend to overestimate flood extent. Interestingly, the AWEI yields a flooded area most similar to that obtained using FMI, which is consistent with its relatively higher Overall Accuracy (OA) reported in Table 1. Similarly, both MNDWI and NDFI produce intermediate estimates that align with their respective OA values (Table 1), further supporting the correspondence between classification accuracy and flood extent estimation.

Figures 4 through 7 provide two details of a spatial comparison between the flood extent detected by each spectral index and the reference classification obtained using the FMI. Areas where the index result matches the FMI classification (true positives - correct) are shown in green. Areas identified by the FMI but missed by the index (false negatives - missed) are highlighted in yellow, while areas classified as flooded by the index but not by the FMI (false positives - false) appear in red.

3.1 NDWI Evaluation

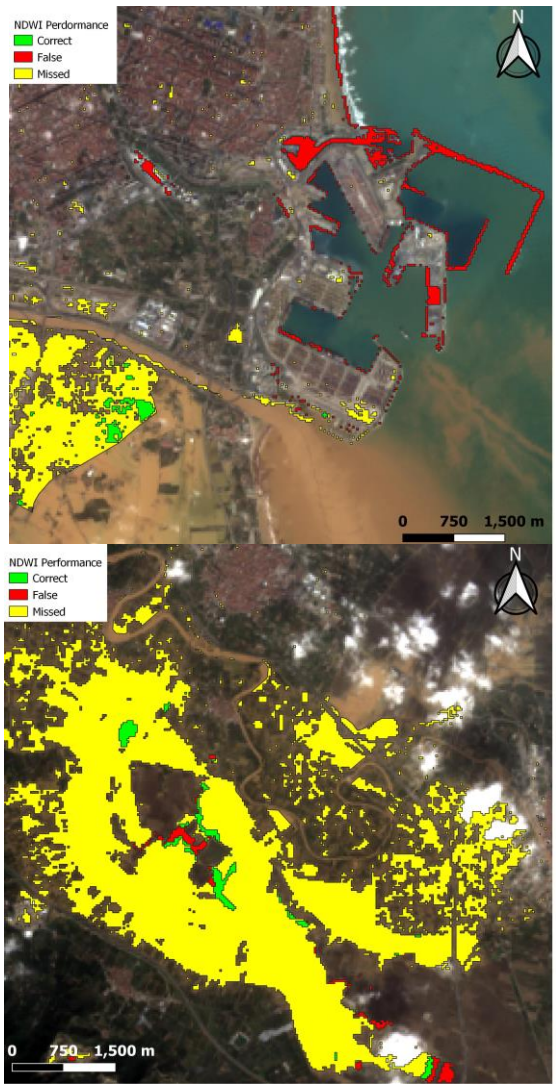

Figure 4. NDWI performance in detecting flooded areas.

Figure 4 reveals that NDWI misses a substantial amount of flooded areas in both the investigated sub-frames. The north frame (on the top) also shows that the port area is incorrectly classified as flooded.

3.2 MNDWI Evaluation

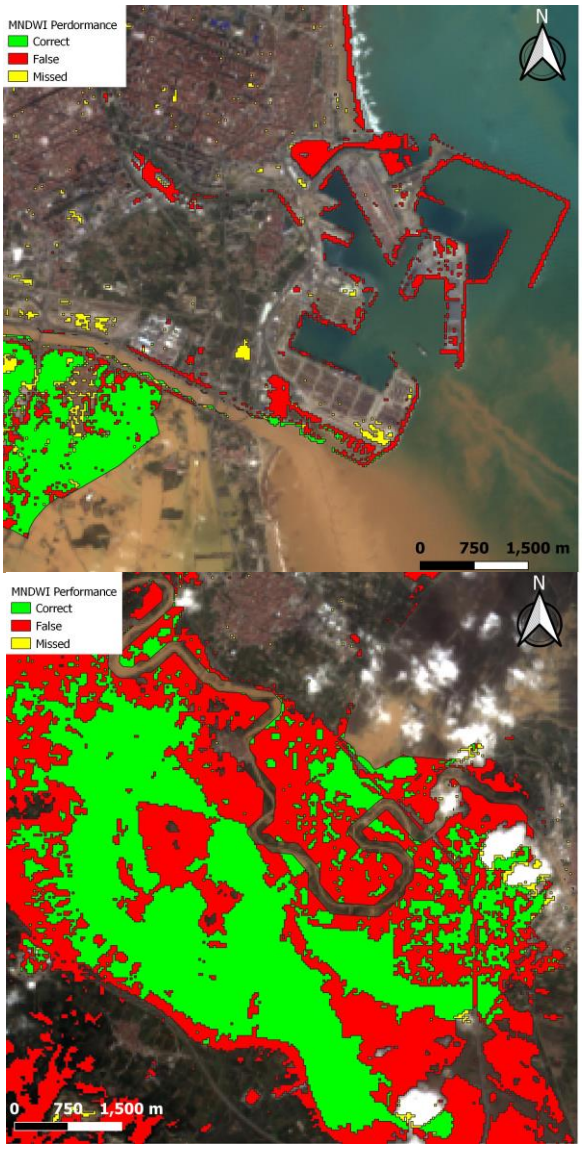

Figure 5. MNDWI performance in detecting flooded areas.

Analysing Figure 5, it is evident that MNDWI highly overestimates the extent of the flooded area in both the northern and southern frames.

3.3 AWEI Evaluation

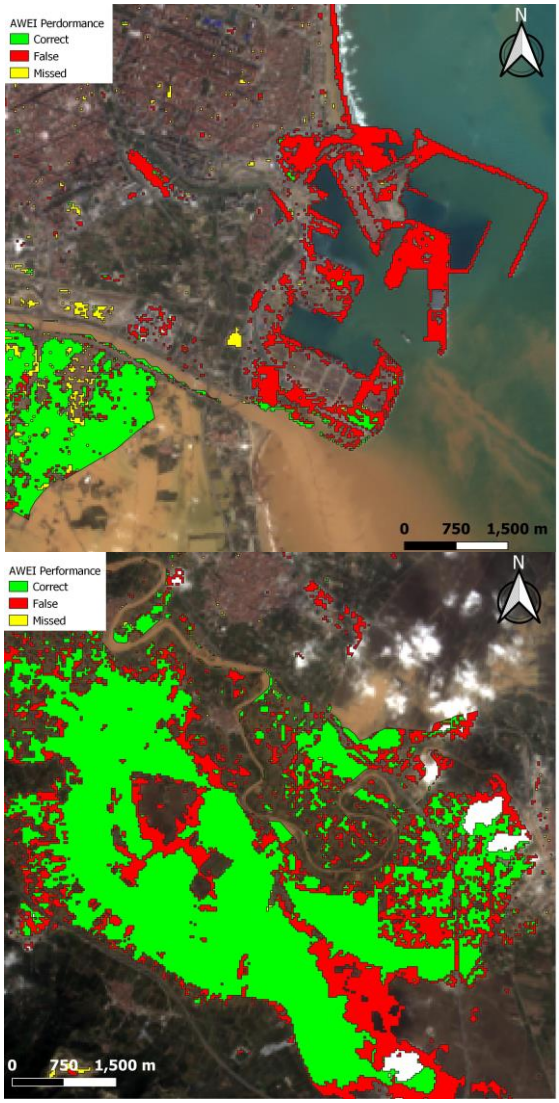

Figure 6. AWEI performance in detecting flooded areas.

As shown in Figure 6, AWEI is the index whose performance is better than the previously analysed ones, especially in the southern frame. However, the port area in the northern frame is highly misclassified (false positive).

3.4 NDFI Evaluation

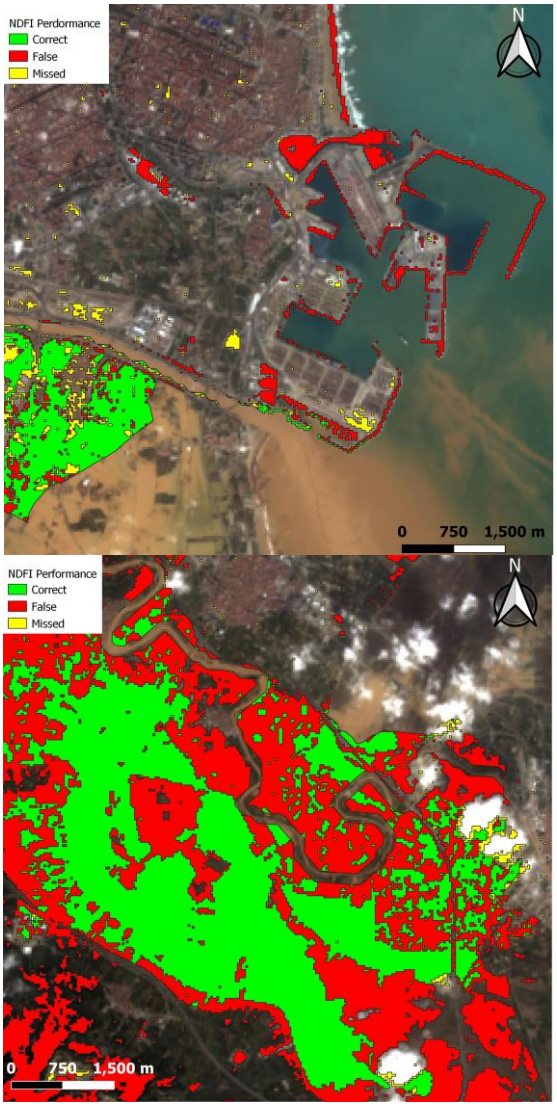

Figure 7. NDFI performance in detecting flooded areas.

As shown in Figure 7, the NDFI overestimate of the flooded areas in the southern frame is very large. Comparing Figure 5 and Figure 7, it seems that NDFI behaviour is similar to that of MNDWI.

3.5 General Considerations

The application of indices other than FMI consistently resulted in the misclassification of port areas as flooded. This issue was observed even with NDWI, which generally underestimates the flood extent but still erroneously identifies several non-flooded regions—including the port—as inundated. This limitation confirms the unsuitability of NDWI for flood detection in this particular context.

Both MNDWI and NDFI behave similarly, tending to significantly overestimate the flooded area. Although they show improved sensitivity to water presence compared to NDWI, they lack precision and introduce considerable commission errors.

Among the tested indices, AWEI performs the best after FMI. However, it still overestimates the extent of flooding. Notably, port infrastructures are heavily misclassified as flooded across all indices. This is likely due to their highly impervious

surfaces, which can exhibit spectral signatures resembling water in certain wavelengths.
While such misclassifications can typically be corrected using bi-temporal analysis (e.g., through pre- and post-event imagery comparison), this approach requires access to suitable pre-event data and additional processing time.
In contrast, the FMI demonstrates strong potential in this context. Its efficiency allows for rapid and reliable mapping of sediment-laden floodwaters using only post-event imagery, making it especially valuable in time-sensitive scenarios or when baseline data are unavailable.

4. Conclusions

This study focused on analysing the severe flood event that struck the Valencian Community in October 2024, with the aim of accurately delineating the extent of the flooded areas. Five spectral indices commonly used in the literature were tested, and the newly proposed FMI emerged as the most effective, achieving an overall accuracy of 97.64% and estimating a flooded area of approximately 4,081.49 hectares.
The goal of the analysis was not only to identify the flood extent with high precision, but also to evaluate the performance of other indices relative to FMI, providing insight into their strengths and limitations in this and potentially similar scenarios. The results showed that NDWI significantly underestimates flood extent in turbid conditions, rendering it unsuitable for this context. Nevertheless, NDWI may still be useful for detecting clearer water bodies with low turbidity.
AWEI performed particularly well, slightly overestimating the flooded area. Given its promising accuracy, future studies will explore the behaviour of AWEI and FMI in other flood scenarios to determine whether their trends align or diverge under different conditions.
It is important to note that the findings presented here are specific to the Landsat 8 OLI dataset and the studied region. Future work will extend this analysis to other geographic areas and satellite sensors to assess the broader applicability and consistency of the tested indices in flood mapping.

References

Aggarwal, A., Rafique, F., Rajesh, E., & Ahmed, S. (2016). Urban flood hazard mapping using change detection on wetness transformed images. *Hydrological Sciences Journal*, *61*(5), 816-825. https://doi.org/10.1080/02626667.2014.952638

Albertini, C., Gioia, A., Iacobellis, V., & Manfreda, S. (2022). Detection of surface water and floods with multispectral satellites. *Remote Sensing*, *14*(23), 6005. https://doi.org/10.3390/rs14236005

Alcaras, E., Amoroso, P. P., Falchi, U., Figliomeni, F. G., Morale, D., & Prezioso, G. (2025, May). Comparative Analysis of Supervised and Unsupervised Classification Methods for Sentinel-2 Imagery. In *2025 5th International Conference on Innovative Research in Applied Science, Engineering and Technology (IRASET)* (pp. 1-6). IEEE. https://doi.org/10.1109/IRASET64571.2025.11007978

Alcaras, E., & Vallario, A. (2025, June). The Role of Pan-Sharpening in Coastline Extraction from High-Resolution Satellite Images. In 2025 IEEE 12th International Workshop on Metrology for AeroSpace (MetroAeroSpace) (pp. 756-761). IEEE. https://doi.org/10.1109/MetroAeroSpace64938.2025.11114587

Alcaras, E. (2025). Flood Mud Index (FMI): A Rapid and Effective Tool for Mapping Muddy Areas After Floods—The Valencia Case. *Remote Sensing*, *17*(5), 770. https://doi.org/10.3390/rs17050770

Argyelan, T., Diez Torrijos, I., Vallés Planells, M. C., & Galiana Galán, F. (2015). Land use change in Huerta de Valencia (2008-2013). Resilience and cultural landscapes. *Irrigation, Society and Landscape. Tribute to Tom F. Glick*, 910-923. http://dx.doi.org/10.4995/ISL2014.2014.201

Astaburuaga, C. R. (2025). Valencia's DANA of October 2024: The 12 days of the state of emergency in the province of Valencia (Spain). *Spanish Journal of Legal Medicine*, 500457. https://doi.org/10.1016/j.remle.2025.500457

Bijeesh, T. V., & Narasimhamurthy, K. N. (2020). Surface water detection and delineation using remote sensing images: A review of methods and algorithms. *Sustainable Water Resources Management*, *6*(4), 68. https://doi.org/10.1007/s40899-020-00425-4

Çal, İ., & Ciravoğlu, A. (2024). Determining Vulnerability Indicators of Buildings for Sea-Level Rise and Floods in Urban Coastal Areas. *Sustainability*, *17*(1), 27. https://doi.org/10.3390/su17010027

Carmona González, P., & Ruiz Pérez, J. M. (2000). Las inundaciones de los ríos Júcar y Turia.

Eguibar, M. Á., Porta-García, R., Torrijo, F. J., & Garzón-Roca, J. (2021). Flood hazards in flat coastal areas of the eastern iberian peninsula: a case study in oliva (Valencia, Spain). *Water*, *13*(21), 2975. https://doi.org/10.3390/w13212975

Feyisa, G. L., Meilby, H., Fensholt, R., & Proud, S. R. (2014). Automated Water Extraction Index: A new technique for surface water mapping using Landsat imagery. *Remote sensing of environment*, *140*, 23-35. https://doi.org/10.1016/j.rse.2013.08.029

Garcia, J. L. M. (2013). The planning of peri-urban agricultural areas: The case of "L'Horta de València".

IPCC. (2022). *Climate Change 2022: Impacts, Adaptation and Vulnerability. Contribution of Working Group II to the Sixth Assessment Report of the Intergovernmental Panel on Climate Change*. Cambridge University Press. https://www.ipcc.ch/report/ar6/wg2/

Liu, X., 2005. Supervised classification and unsupervised classification. ATS 670 Class Project.

Liu, C., Frazier, P., & Kumar, L. (2007). Comparative assessment of the measures of thematic classification accuracy. *Remote sensing of environment*, *107*(4), 606-616. https://doi.org/10.1016/j.rse.2006.10.010

Mianji, F. A., & Zhang, Y. (2011). Robust hyperspectral classification using relevance vector machine. IEEE Transactions on Geoscience and Remote Sensing, 49(6), 2100-2112. https://doi.org/10.1109/TGRS.2010.2103381

Martin-Moreno JM, Garcia-Lopez E, Guerrero-Fernandez M, Alfonso-Sanchez JL and Barach P (2025) Devastating "DANA" Floods in Valencia: Insights on Resilience, Challenges, and

Strategies Addressing Future Disasters. Public Health Rev. 46:1608297. https://doi.org/10.3389/phrs.2025.1608297

McFeeters, S. K. (1996). The use of the Normalized Difference Water Index (NDWI) in the delineation of open water features. *International journal of remote sensing*, *17*(7), 1425-1432. https://doi.org/10.1080/01431169608948714

Morote, Á. F., Tévar, B., & Olcina, J. (2025). The 2024 Floods in Valencia (Spain): Case Study of Flood Risk Education in a Primary Education Setting. *GeoHazards*, *6*(2). https://doi.org/10.3390/geohazards6020030

Moya, L., Endo, Y., Okada, G., Koshimura, S., & Mas, E. (2019). Drawback in the change detection approach: False detection during the 2018 western Japan floods. *Remote Sensing*, *11*(19), 2320. https://doi.org/10.3390/rs11192320

Munawar, H. S., Hammad, A. W., & Waller, S. T. (2021). A review on flood management technologies related to image processing and machine learning. *Automation in Construction*, *132*, 103916. https://doi.org/10.1016/j.autcon.2021.103916

Munawar, H. S., Hammad, A. W., & Waller, S. T. (2022). Remote sensing methods for flood prediction: A review. *Sensors*, *22*(3), 960. https://doi.org/10.3390/s22030960

Muñoz-Marí, J., Bruzzone, L., Camps-Valls, G., 2007. A support vector domain description approach to supervised classification of remote sensing images. *IEEE Transactions on Geoscience and Remote Sensing*, 45(8), 2683-2692. https://doi.org/10.1109/TGRS.2007.897425

Nissen, K. M., & Ulbrich, U. (2017). Increasing frequencies and changing characteristics of heavy precipitation events threatening infrastructure in Europe under climate change. *Natural Hazards and Earth System Sciences*, *17*(7), 1177-1190. https://doi.org/10.5194/nhess-17-1177-2017

Perumal, K., Bhaskaran, R., 2010. Supervised classification performance of multispectral images. *Journal of computing*, 2(2), 124-129.

Quantum GIS – User Manual, 2025. https://docs.qgis.org/3.40/it/docs/user_manual/index.html

Rahman, M. S., & Di, L. (2017). The state of the art of spaceborne remote sensing in flood management. *Natural Hazards*, *85*(2), 1223-1248. https://doi.org/10.1007/s11069-016-2601-9

Ramola, A., & Vidyarthi, A. (2024, June). Analysing Distinct Change Detection Methods for Identifying Spectral and Spatial Variation Using Planetscope Satellite Data. In *2024 International Conference on Integrated Circuits, Communication, and Computing Systems (ICIC3S)* (Vol. 1, pp. 1-6). IEEE. https://doi.org/10.1109/ICIC3S61846.2024.10602864

Rencz, A. N., & Ryerson, R. A. (Eds.). (1999). *Manual of remote sensing, remote sensing for the earth sciences*. John Wiley & Sons.

Richards J.A., 2013. Supervised Classification Techniques, in: *Remote Sensing Digital Image Analysis*. Springer, Berlin, Heidelberg. https://doi.org/10.1007/978-3-642-30062-2_8

Samela, C., Coluzzi, R., Imbrenda, V., Manfreda, S., & Lanfredi, M. (2022). Satellite flood detection integrating hydrogeomorphic and spectral indices. *GIScience & Remote Sensing*, *59*(1), 1997-2018. https://doi.org/10.1080/15481603.2022.2143670

Sisodia, P.S., Tiwari, V., Kumar, A., 2014. Analysis of supervised maximum likelihood classification for remote sensing image. In: *International conference on recent advances and innovations in engineering (ICRAIE-2014),* IEEE, 1-4. https://doi.org/10.1109/ICRAIE.2014.6909319

Soria, J., Vera-Herrera, L., Calvo, S., Romo, S., Vicente, E., Sahuquillo, M., & Sòria-Perpinyà, X. (2021). Residence time analysis in the albufera of Valencia, a Mediterranean Coastal Lagoon, Spain. *Hydrology*, *8*(1), 37. https://doi.org/10.3390/hydrology8010037

Story, M., & Congalton, R. G. (1986). Accuracy assessment: a user's perspective. *Photogrammetric Engineering and remote sensing*, *52*(3), 397-399.

Teillet, P. M., Staenz, K., & William, D. J. (1997). Effects of spectral, spatial, and radiometric characteristics on remote sensing vegetation indices of forested regions. *Remote Sensing of Environment*, *61*(1), 139-149. https://doi.org/10.1016/S0034-4257(96)00248-9

U.S. Geological Survey, Landsat 8 (L8) Data Users Handbook – Version 5.0. November 2019. https://d9-wret.s3.us-west-2.amazonaws.com/assets/palladium/production/s3fs-public/atoms/files/LSDS-1574_L8_Data_Users_Handbook-v5.0.pdf [Accessed on 20 July 2025].

Wan, K. M., & Billa, L. (2018). Post-flood land use damage estimation using improved Normalized Difference Flood Index (NDFI3) on Landsat 8 datasets: December 2014 floods, Kelantan, Malaysia. *Arabian Journal of Geosciences*, *11*(15), 434. https://doi.org/10.1007/s12517-018-3775-0

Xu, H. (2006). Modification of normalised difference water index (NDWI) to enhance open water features in remotely sensed imagery. *International journal of remote sensing*, *27*(14), 3025-3033. https://doi.org/10.1080/01431160600589179